International Journal of Concrete Structures and Materials

RESEARCH Open Access

Anti-explosion Performance of a New Type of Polyurea-Coated Corrugated Steel Plate Reinforced Concrete Slab

Wei Wang[1,2*], Congkun Zhang[1] and Guangrui Yang[1]

Abstract

Improving the explosion resistance of the building wall has been a hot topic in the current protection engineering research, in this process, corrugated steel and polyisocyanate oxazolidine (POZD) were widely used, but there are few studies on the anti-explosion performance of the composite structure of the two. In this paper, the effects of POZD and corrugated steel on the explosion resistance of POZD-coated corrugated steel plate reinforced concrete slab (PSRC) under contact explosion were studied by test and numerical simulation. The finite element (FE) model of the PSRC slab was established by using Arbitrary Lagrangian–Eulerian (ALE) method. The principle of POZD coating reinforced structure was revealed by analyzing the attenuation process of stress wave propagation in the structure. Subsequently, a series of numerical calculations were conducted to investigate the effect of POZD thickness and corrugated steel angle on the performance of the PSRC slab under explosive load. The relationship between structural damage characteristics and the POZD coating was established, the empirical formula of the normalized maximum mid-span displacement considering POZD thickness and TNT mass was obtained. The effect of corrugated steel with different angles on its anti-explosion performance was analyzed, the empirical formula of the maximum deflection considering corrugated steel angle and TNT mass was obtained. Studies have shown that the peak stress of the stress wave generated by the explosion is only 2.79% of the incident wave after the POZD coating is coated on the back of the structure, the anti-explosion performance of the structure is greatly improved. Increasing the thickness of POZD can significantly increase the anti-explosion performance of PSRC slab, the maximum deflection of PSRC slab decreases exponentially with increasing POZD thickness. The explosion resistance of PSRC slab was enhanced with increasing corrugated steel angles. The corrugated steel angles is 50 , the improvement effect of PSRC is the best.

Keywords Contact explosion, Numerical simulation, Damage effect

1 Introduction

With the rampant terrorism, the explosions caused by terrorist attacks are increasing worldwide, and the safety of people's lives and property has been seriously threatened (Li et al., 2016; Shi et al., 2008, 2020; Yong et al., 2005). Such as the explosion of hazardous chemicals in Hebei Province in November 2018 and the explosion of ammonium nitrate in Beirut, Lebanon in October 2020, have caused serious damage to local buildings. Therefore, improving the explosion resistance of the building wall has been a hot topic in the current protection

Journal information: ISSN 1976-0485 / eISSN 2234-1315.

*Correspondence:
Wei Wang
wangwei7@nbu.edu.cn
[1] Key Laboratory of Impact and Safety Engineering, Ministry of Education, Ningbo University, Ningbo 315211, Zhejiang, China
[2] Institute of Advanced Energy Storage Technology and Equipment, Ningbo University, Ningbo 315211, Zhejiang, China

engineering research (Wang et al., 2012, 2013a, 2013b, 2014; Wang et al. 2023).

Polyurea elastomer is a special polymer material, it has excellent impact resistance and ductility (Arman et al., 2012; Haris et al., 2018; Iqbal et al. 2018). Coating polyurea on concrete surface can effectively reduce the risk of structural deformation and delamination (Wu et al. 2021). Therefore, polyurea elastomer is often used in protective coating of protective engineering. (Gu et al., 2022) synthesized five polyurea elastomers by changing composition of isocyanate. The research results showed that polyurea could significantly improve the anti-blast performance. Increasing the thickness of the polyurea on the backside can further improve the anti-blast performance. Through explosion test and numerical simulation, (Liu et al., 2022a, 2022b, 2022c) investigated the enhancement effectiveness of polyurea on the anti-explosion performance of RC slabs under near-field explosion. (Liu et al., 2022a, 2022b, 2022c) conducted two scale tests to study the effect of polyurea coating on the anti-explosion performance of hull. The results showed that polyurea has a better blast resistance performance when coated on the blast-facing surface of the steel plate. (Shi et al., 2019) conducted explosion experiments on polyurea woven carbon fiber mesh composite reinforced RC slabs. The results showed that polyurea coating can reduce the threat area caused by concrete fragments caused by explosions. (Wang et al., 2022a, 2022b, 2022c) studied the anti-explosion performance of RC slab strengthened with polyisocyanate oxazolidine (POZD) coated steel plate, analyzed the damage mechanism and divided the damage mode and the results showed that increasing the thickness of POZD can effectively reduce the POZD–steel–RC slab mid-span deflection (Zhang et al., 2022) studied the protective ability of polyurea-coated steel plates under blasting through field tests, the results showed only when the coating thickness exceeded a certain value did polyurea play a strengthening role (Zhu et al., 2022) revealed the damage behavior of masonry walls reinforced by polyurea double-sided at different explosion distances, it was found that polyurea sprayed on the rear face was better than on the front face, and the effect of double-sided coating was best at the same blast scaled distance.

In general, increasing the polyurea thickness can improve the anti-explosion performance. However, considering the cost reasons, it is unrealistic to infinitely increase the polyurea coating thickness. Therefore, it is a good choice to spray polyurea on corrugated steel to form composite structure. On the one hand, corrugated steel can provide large out-of-plane stiffness, which is conducive to enhancing the bending strength and stiffness of the structure (Yang et al., 2021; Zhang et al., 2021). On the other hand, polyurea has good ductility and plastic deformation ability.

At present, (Li et al., 2022) conducted tests on the compression performance of double-layer corrugated steel composite wall filled with concrete, established a FE model for further study and proposed calculation formulas of compressive strength and axial compression resistance of composite wall (Sun et al., 2022) investigated the constraint mechanism of corrugated steel tube confined column core concrete, analyzed the influence of section size, steel tube width, corrugated steel plate wave height and thickness on core concrete strength index and specimen ductility index. Through experiments and numerical simulations, (Zuo et al., 2022) found that steel corrugated plate coupling beams had high shear capacity. (Wang et al., 2022a, 2022b, 2022c) developed the multi-grid corrugated steel shear wall, found its out-of-plane stiffness is further improved compared with ordinary corrugated steel plate shear wall. (Ghodratian-Kashan & Maleki, 2022) conducted experimental research and simulation verification on cyclic performance of double corrugated steel plate shear wall and discovered spindle-shaped hysteresis curves with good cyclic performance. At present, many researches on corrugated steel have been done, but there are few researches on the dynamic response at high strain rate.

In order to qualitatively and quantitatively study the damage effect and anti-explosion performance of POZD-coated corrugated steel reinforced concrete slabs under explosion load. In the paper, the explosion resistance of PSRC slab was studied by test and numerical simulation. The damage characteristics of PSRC slab were analyzed, the FE model was established and verified with the test results. On this basis, a series of numerical calculations were conducted using the verified finite element model to investigate the effects of POZD thicknesses and corrugated steel angles on performance of PSRC slab under explosive loading. The relationship between the quantitative damage characteristics and POZD thickness was established by dimensionless analysis, the empirical formula of the normalized damage characteristics considering the POZD thickness and TNT mass was obtained. The effects of different angles of corrugated steel on the anti-explosion performance of the structure were analyzed.

2 Methodology and Materials

To investigate the explosion resistance of PSRC slab, this study combined field tests and numerical model. This section describes how to conduct contact explosion tests, establish numerical models, and compare them with experimental results to verify the effectiveness of the finite element model. Based on the above contents,

the numerical model could be extended to study the anti-explosion performance of PSRC slab under contact explosion loads.

2.1 Experimental Conditions

The specimen was constructed. It can be seen from Fig. 1 that the specimen consists of a concrete slab, corrugated steel plate and POZD coating. The geometrical dimensions of the whole configuration were 2000 mm × 2000 mm × 315 mm (length × width × thickness). The specimens were poured with C40 (The compressive strength of standard cube specimens is greater than or equal to 40 MPa concrete) concrete, in which the compressive strength was 41.2 MPa after curing for 28 days. The HRB400 (Hot-rolled Ribbed Bar with yield strength of 400 MPa) steel was used for the rebar. The rebar reinforcement Φ14@200 × 200 is arranged in two layers. Corrugated steel used Q235 steel with a thickness of 3 mm, a wave height of 165 mm, and a wave crest distance of 300 mm. POZD is a polyurea-based polymer material with better tensile and tear properties than polyurea as shown in Fig. 2. The thickness of POZD is 12 mm. The tensile strength of POZD is more than 25 MPa and the shear strength is more than 85 kN/m, these properties have been investigated in Ref (Wang et al., 2021).

Fig. 3 displays the layout of the field test. The specimen was placed on the steel frame and the wave crest at the bottom of the model was tangent to the beam of the steel frame. The four boundaries of the model were fixed on the steel frame by using G-clamps. The bottom of the model was suspended to simulate the vacant state of the structure, the anti-explosion performance was judged by observing the damage characteristics to the bottom. Table 1 demonstrates the specific test program.

The mass of a single explosive is 200 g, the geometrical dimensions are 300 mm × 50 mm × 25 mm (length × width × thickness). The charge used in the tests was an integer multiple of 200 g, as shown in Fig. 4. TNT explosive was fixed into an approximate cube by the

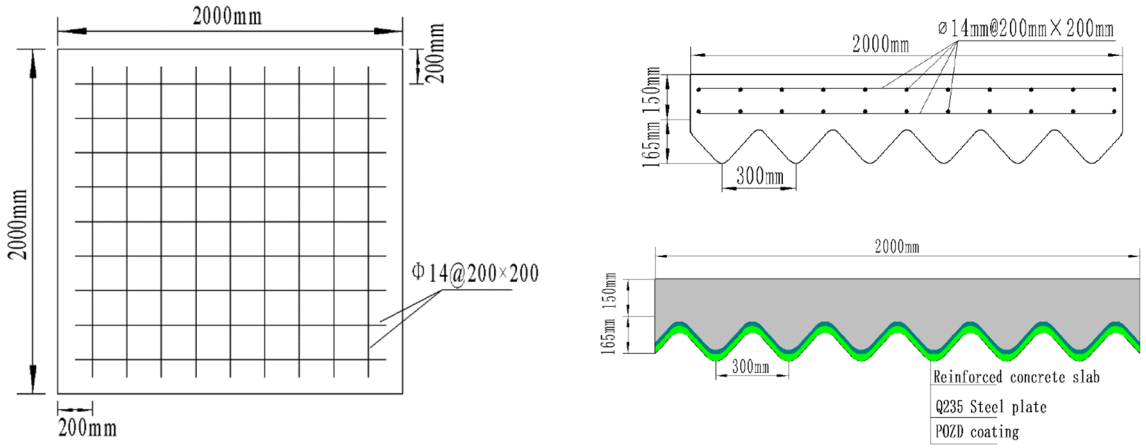

Fig. 1 Geometry and reinforcement of specimen

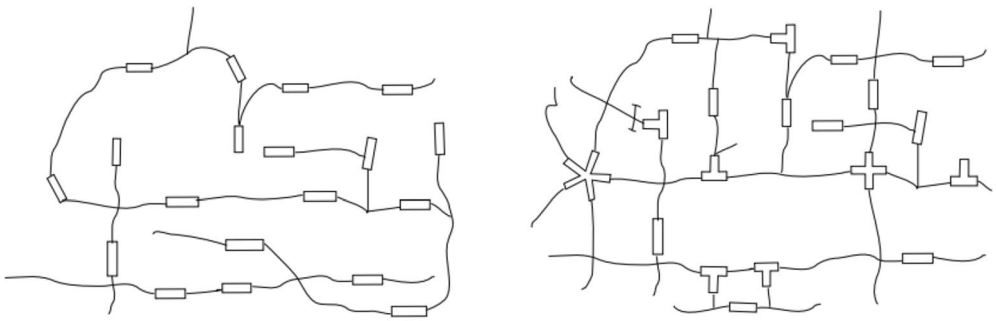

Fig. 2 Network structure of polyuria and POZD

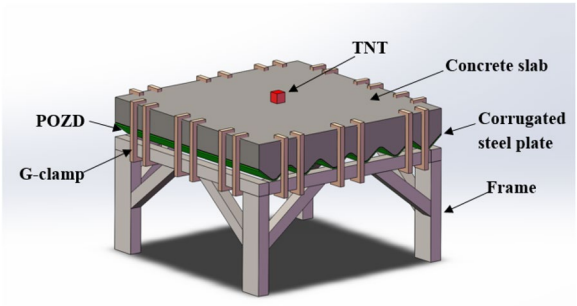

Fig. 3 Test device

Table 1 Test program

Case	Specimen	Concrete thickness (mm)	Steel plate thickness (mm)	POZD thickness (mm)	TNT (g)
1	PSRC	315	3	12	4000

transparent tape and the explosive source was placed on the specimen.

2.2 FE Model

Contact explosion is an extremely complex process and the dynamic response time is very short (Xu et al., 2022). Researchers often use the multi-material arbitrary Lagrangian–Eulerian (ALE), smoothed particle hydrodynamics (SPH) and particle blast method (PBM) methods for numerical simulation. However, SPH method can cause dispersion and instability of explosive load and PBM method cannot define the state equation of explosive (Chilvers et al., 2022). In this paper, the ALE method was used to simulate the dynamic response of the structure under explosion load in ANSYS/LS-DYNA software.

The numerical operation flow is shown in Figs. 5. 6 presents the FE model of PSRC slab. The air is modeled by 3D solid elements, the grid size is 20 mm. Bar is modeled by beam elements, the grid size is 10 mm. Concrete, steel plate, POZD and TNT are modeled by

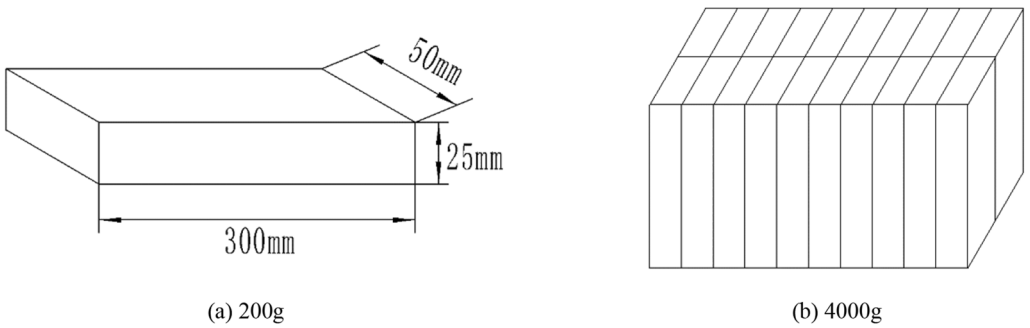

(a) 200g (b) 4000g

Fig. 4 The shape and size of TNT

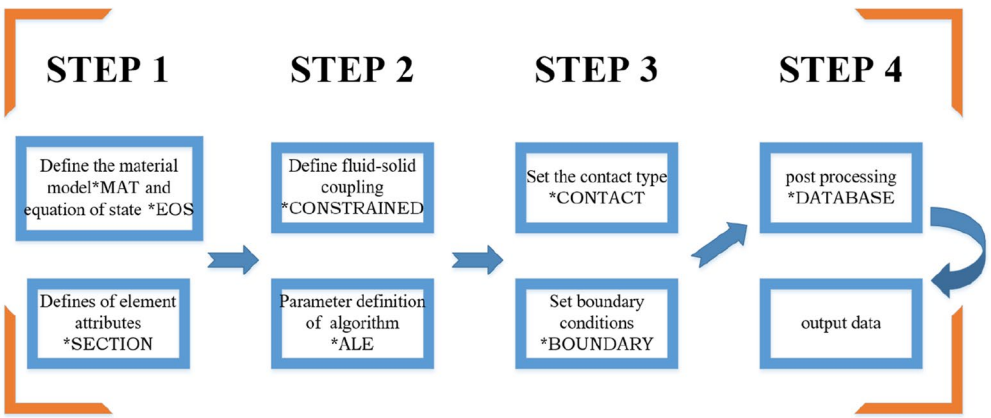

Fig. 5 Numerical operation flowchart

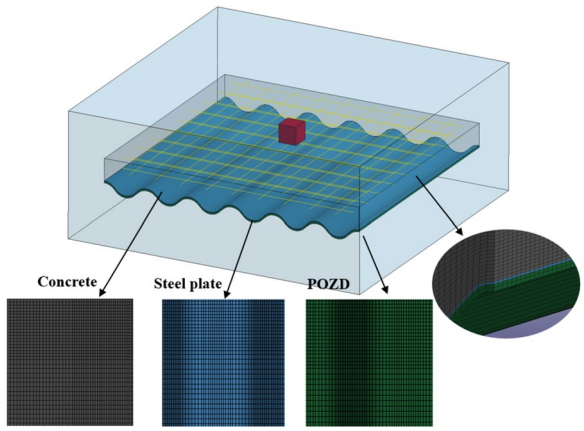

Fig. 6 FE model and meshing

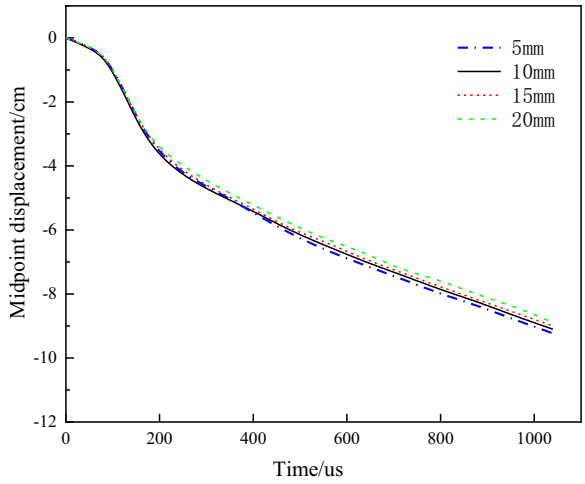

Fig. 7 Convergence analysis

3D solid elements. Considering time cost and simulation accuracy, the mesh size of concrete, steel plate and POZD are partially encrypted. In order to ensure that the numerical simulation results were not affected by the mesh size, the mesh size of the model was analyzed for convergence. The element meshes were taken as 5, 10, 15 and 20 mm, respectively, to calculate the maximum deflection of the PSRC slab, and the displacement curves were obtained as shown in Fig. 7. The peak displacements were 92.3, 91.0, 90.0 and 88.9 mm for mesh sizes 5, 10, 15 and 20 mm, with errors of 1.4%, 0, 1.1% and 2.3% for mesh size 10 mm. For the purpose of ensuring mesh convergence and saving computational resources, the mesh size near TNT and the mesh size of structural boundary were finally taken as 10 mm and 20 mm, the counts for structural and air model elements were 5536135. Use the keywords CONTACT_AUTOMATIC_SURFACE_TO_SURFACE to define the adhesive force between concrete and steel plate, steel plate and POZD. In addition, the keywords MAT_ADD_ERROSION was used to describe severe damage processes. (Li & Hao, 2014) found that using 0.01 principle tensile strain as the erosion criterion can reliably predict the response of RC slabs. Therefore, 0.01 was selected as the erosion criterion in this paper, it can well describe the damage of slab.

2.3 Material Model

MAT_CONCRETE_DAMAGE_REL3 was selected as the material model of concrete. It is the third version based on Karagozian and Case model (Liu et al., 2022a, 2022b, 2022c). The model has three shear failure surfaces, it can be based on the default parameter generation function of infinite compressive strength of concrete (Erduran & Yakut, 2004; Malvar et al., 1997). The unconfined compressive strength after curing 28 days was 41.2 MPa in this paper.

The MAT_PLASTIC_KINEMATIC was used for steel plate and steel bar. Strain rate was accounted for using the Cowper and Symonds model which scales the yield stress with the factor as follows(Zhao et al., 2019):

$$\sigma_y = 1 + \left(\frac{\dot{\varepsilon}}{C}\right)^{\frac{1}{P}} \tag{1}$$

σ_y denotes yield stress; $\dot{\varepsilon}$ denotes the strain rate; C and P are the coefficients in model. In this paper, σ_y of the steel plate is 235 MPa, σ_y of the steel bar is 400 MPa, C and P are 13.8 S^{-1} and 5.

The stress–strain behavior of POZD is highly dependent on strain rate. The US Air Force Laboratory had measured the stress curves of polyurea under different strain rates (Davidson, Sudame et al. 2004). The MAT_PIECEWISE_LINEAR_PLASTICITY was adopted to represent the tensile and compressive behavior of POZD. According to the research done in Ref. (Wang et al., 2022a, 2022b, 2022c), the tensile failure of POZD was defined as 0.85.

The air was modeled with the Null material model as an ideal gas (Cheng et al., 2019; Song et al., 2016). The EOS_LINEAR_ POLYNOMIAL was used to simulate the equation of state of the air as follow (Liu et al., 2022a, 2022b, 2022c):

$$P = C_0 + C_1\mu + C_2\mu^2 + C_3\mu^3 + (C_4 + C_5\mu + C_6\mu^2)E_0. \tag{2}$$

P denotes the pressure; E_0 denotes initial internal energy per unit volume; $C_0 - C_6$ denotes the coefficients; $\mu = \frac{1}{V} - 1$, where V is the relative volume. In this paper, $C_0 = C_1 = C_2 = C_3 = C_6 = 0$, $C_4 = C_5 = 0.4$, $E_0 = 0.25J/m^3$.

The MAT_HIGH_EXPLOSIVE_BURN was selected for TNT charge (Wu et al., 2021). Its corresponding equation of state is as follows:

$$P_{cj} = A_1(1 - \frac{\omega}{R_1 V})e^{-R_1 V} + B_1(1 - \frac{\omega}{R_2 V})e^{-R_2 V} + \frac{\omega e_0}{V}, \quad (3)$$

where P_{cj} denotes the pressure; A_1, B_1, R_1, R_2 and ω denote the coefficients of the explosion; e_0 denotes the initial internal energy per unit volume; V denotes the relative volume. In this paper, $P_{cj} = 21000MPa$; $e_0 = 7.0MJ \cdot \mathrm{Kg}^{-1}$; V=1; A_1= 3.71×10^{11}; B_1=3.29×10^9; R_1=4.15; R_2=0.95; ω=0.3.

3 Results and Discussion

3.1 Results and Verification

The damage deformation of PSRC slab is demonstrated in Fig. 8. In numerical simulation, a 323-mm-diameter crater was created on the front, slightly larger than that measured in the experiment, as shown in Fig. 8(a). The damage on the back numerically was elliptical bulge deformation, which was the same as the experimental result. In the simulation, the bulge long diameter was 997 mm, the bulge short diameter was 376 mm, which were similar to the 963 mm and 352 mm measured in the experiment, as shown in. Fig. 8(b). Comparing the numerical simulation results with the experimental results, the error of the crater diameter is 10.8%, and the errors of the bulge long diameter and bulge short diameter are 3.5% and 6.8%, respectively. The numerical simulation results were reasonable compared with the experimental results.

3.2 Damage Characteristic Response Analysis

The deformation and damage process of PSRC specimen under 4000 g TNT explosive are demonstrated in Fig. 9. At about 79 ms, at the front of the specimen, the concrete medium generated crater under the blast wave, and the back concrete had slight cracks. At about 239 ms, due to the poor tensile strength of the concrete medium, the back of concrete slab produced spalling, POZD-coated steel plate produced slight bulging deformation. At about 719 ms, the spalling on the back of concrete continued to expand and the crack spreads around, the bulging

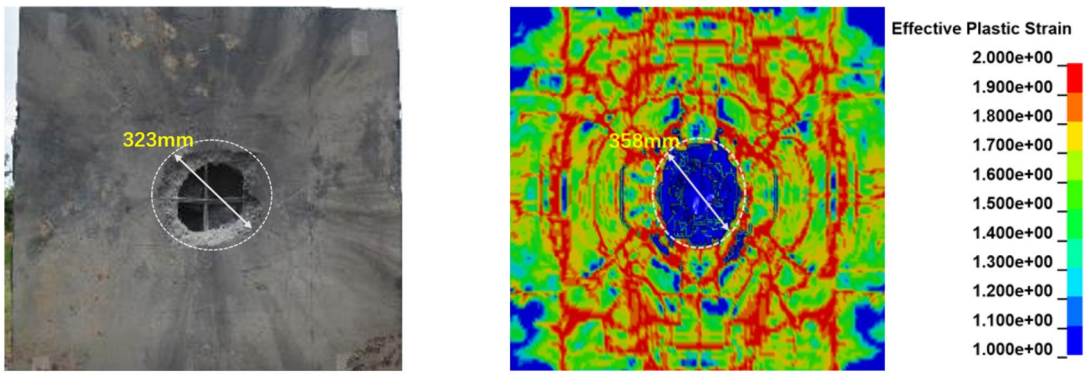

(a) Front face

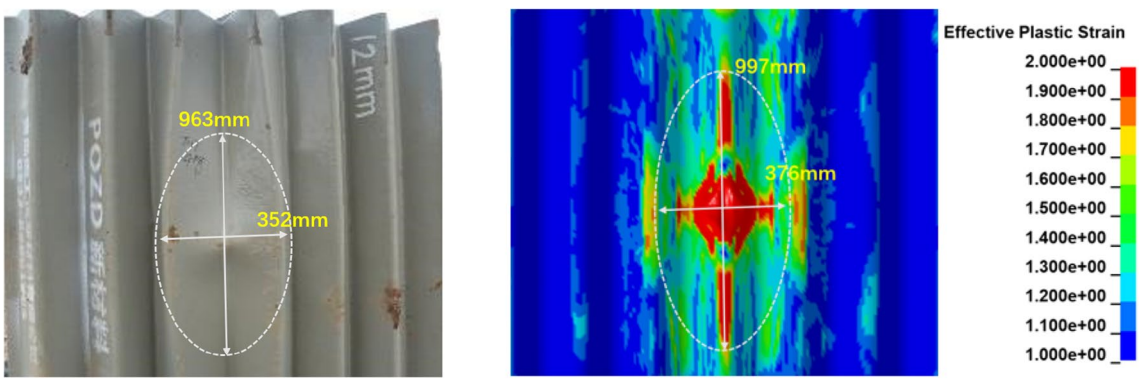

(b) Back face

Fig. 8 Damage comparison of PSRC. **a** Front face. **b** Back face

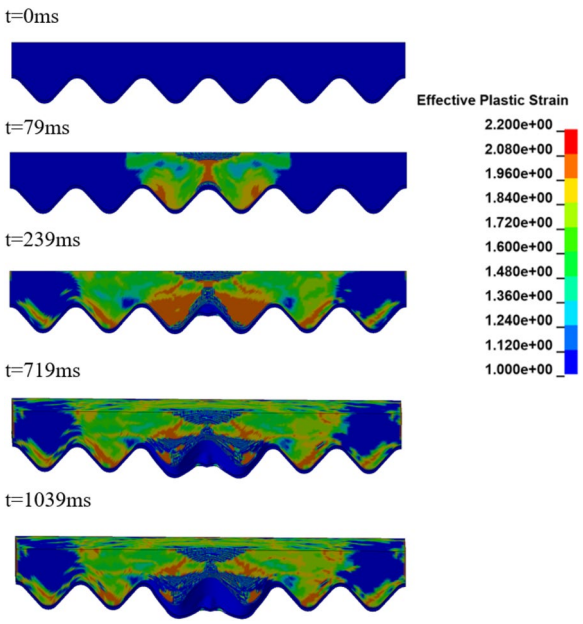

Fig. 9 Deformation and damage process of PSRC

deformation area increased. At about 1039 ms, the whole concrete slab was destroyed, and the back concrete was stripped, and the bulge of POZD-coated corrugated steel continued to expand outward. Then, due to the high ductility and energy absorption of POZD, the damage morphology of PSRC specimen remained stable.

3.3 Structural Theory Analysis

It is assumed that the concrete medium and the steel plate medium are always in contact at the intersection, and no detachment occurs. According to Newton's third law and continuity condition, the incident wave $\triangle \sigma_I$ is reflected and refracted through the concrete slab at the intersection of the concrete medium and the steel plate medium, and the velocity and stress of the masses on both sides are the same, which can be obtained as follows:

$$\triangle v_I + \triangle v_R = \triangle v_T, \tag{4}$$

$$\triangle \sigma_I + \triangle \sigma_R = \triangle \sigma_T. \tag{5}$$

$\triangle v_I$ denotes the wave speed of the incident wave, $\triangle v_R$ denotes the wave speed of the reflected wave, $\triangle v_T$ denotes the wave speed of the transmitted wave; $\triangle \sigma_I$ denotes the stress of the incident wave, $\triangle \sigma_R$ denotes the stress of the reflected wave, $\triangle \sigma_T$ denotes the stress of the transmitted wave.

According to the law of conservation of energy, the relationship between the mass velocity and stress on both sides of the intersection can be obtained, where the left side of the equation represents the mass velocity and stress in the concrete medium, and the right side of the equation represents the mass velocity and stress in the steel plate medium (Wu et al. 2021):

$$\begin{cases} \triangle \sigma_R = F \triangle \sigma_I \\ \triangle v_R = -F \triangle v_I \end{cases}, \tag{6}$$

$$\begin{cases} \triangle \sigma_T = T \triangle \sigma_I \\ \triangle v_T = nT \triangle v_I \end{cases}, \tag{7}$$

$$\begin{cases} n = (\rho_1 C_1)/(\rho_2 C_2) \\ F = (1-n)/(1+n) \\ T = 2/(1+n) \end{cases}. \tag{8}$$

F denotes the reflection coefficient of stress wave, T denotes the transmission coefficient of stress wave, n denotes the ratio of wave impedance of concrete medium and steel plate, ρ_1 denotes the density of concrete medium, C_1 denotes the wave velocity of concrete material, $\rho_1 C_1$ denotes the wave impedance of concrete medium, ρ_2 denotes the density of corrugated steel medium, C_2 denotes the wave velocity of corrugated steel medium, $\rho_2 C_2$ denotes the wave impedance of corrugated steel medium.

The transmission coefficients T and reflection coefficients F satisfy the following relationship:

$$T = 1 + F. \tag{9}$$

According to Zhenyu Han (Han et al. 2020), the direction of the transmitted wave $\triangle \sigma_T$ is often the same as that of the incident wave $\triangle \sigma_I$, so the transmission coefficient T is always positive, while the direction of the reflected wave $\triangle \sigma_R$ is not determined, so the positive or negative reflection coefficient F is not determined, depending on the magnitude of the wave impedance ratio n. According to the ratio of wave impedance n, the magnitude of the transmission coefficient T and the positive or negative reflection coefficient F, there are three cases:

(1) The ratio of wave impedance $n > 1$, reflection coefficient $F < 0$, transmission coefficient $T < 1$.
(2) The ratio of wave impedance $n < 1$, reflection coefficient $F > 0$, transmission coefficient $T > 1$.
(3) The ratio of wave impedance $n = 1$, reflection coefficient $F = 0$, transmission coefficient $T = 1$.

When the stress wave was transmitted from the concrete medium to the corrugated steel medium, it is a process from a medium with low wave impedance to a medium with high wave impedance, and the peak stress of the transmitted wave $\triangle \sigma_T$ in the corrugated steel plate can be obtained as:

$$\triangle \sigma_T = \frac{2\rho_2 C_2}{\rho_1 C_1 + \rho_2 C_2} \triangle \sigma_I. \tag{10}$$

$\rho_1 C_1$ is the wave impedance of concrete, the average value is taken as 7.2 $MPa/m \cdot s$; $\rho_2 C_2$ is the wave impedance of corrugated steel medium, the average value is 39 $MPa/m \cdot s$, which gives:

$$\triangle \sigma_T = \frac{2\rho_2 C_2}{\rho_1 C_1 + \rho_2 C_2} \triangle \sigma_I = 1.688 \triangle \sigma_I. \tag{11}$$

After the POZD was coated on the back side of the corrugated steel plate, $\triangle \sigma_I$ passed through the concrete medium to form $\triangle \sigma_T$ in the steel medium, and $\triangle \sigma_T$ would continue to transmit and reflect through the intersection of the corrugated steel plate and the POZD coating. In the actual composite structure, an adhesive layer exists between the POZD coating and the corrugated steel. To simplify the analysis process, this interfacial adhesive layer was neglected. It was assumed that under the impact of the blast load, the adhesive force between the two medium is always present and the two medium are not separated. Therefore, when the stress wave propagates at the intersection of corrugated steel and POZD coating, it is a process of high wave impedance medium to low wave impedance medium, and the peak stress of transmitted wave $\triangle \sigma_{T2}$ in the POZD coating can be obtained as:

$$\triangle \sigma_{T2} = \frac{2\rho_3 C_3}{\rho_2 C_2 + \rho_3 C_3} \triangle \sigma_T. \tag{12}$$

$\rho_2 C_2$ is the wave impedance of the corrugated steel medium with an average value of 39 $MPa/m \cdot s$, $\rho_3 C_3$ is the wave impedance of the POZD coating with an approximate value of 0.326 $MPa/m \cdot s$, which gives:

$$\triangle \sigma_{T2} = \frac{2\rho_3 C_3}{\rho_2 C_2 + \rho_3 C_3} \triangle \sigma_T = 0.0165 \triangle \sigma_T = 0.0279 \triangle \sigma_I. \tag{13}$$

We can see that the structure was coated with POZD coating behind the structure, so that the stress wave generated by the explosion through the concrete medium, steel plate medium and POZD coating medium, the peak stress is only 2.79% of the incident wave, which greatly weakened the energy propagation of the stress wave and better improved the protective performance of corrugated steel reinforced concrete slab.

4 Parametric Studies

The numerical results of the third section showed that the developed FE model conformed to the dynamic response process of PSRC slab. To explore the factors affecting the anti-explosion performance, the parametric analysis was carried out by changing POZD thickness, TNT mass and corrugated steel angle.

4.1 Influence of POZD Thickness

Through 334 blast tests, McVay(Mcvay) found that the damage characteristics of concrete structures are related to $R/W^{1/3}$ and $T/W^{1/3}$, where R represents the detonation center height, T represents the structural thickness, and W represents the TNT charge. $R/W^{1/3}$ often used to evaluate the damage effect of air blast resistance of structures, while $T/W^{1/3}$ is used to evaluate the damage effect under contact explosion. (Liu et al., 2022a, 2022b, 2022c) and (Wang et al., 2022a, 2022b, 2022c) studied the relationship between $R/W^{1/3}$ and structural damage characteristics through experiments and numerical simulations. (Ichino et al., 2020); (Yu et al., 2020) and (Masahiro et al., 2004) divided the damage modes under different charges by $T/W^{1/3}$. Based on this study, the effect of POZD thickness and TNT mass on blast resistance was further explored in this paper.

In this section, 6 mm, 12 mm and 16 mm POZD coatings are coated on the RC slabs strengthened with corrugated steel, respectively, the TNT charge varies from 500 to 7000 g and the other parameters are the same as the above finite element simulation results. The numerical results are listed in Table 2. Taking the maximum deflection on the back as the damage characteristics, POZD thickness and TNT mass were used as factors affecting the blast resistance. Dimensionless treatment of maximum deflection and POZD thickness, as shown in Fig. 10. where l represents the maximum deflection of the structure, h represents POZD coating thickness, T represents total slab thickness and W represents TNT mass.

Fig. 10 illustrates the relationship between the maximum deflection and TNT mass, POZD thickness. When POZD thickness is constant, the maximum deflection of the structure increases with increasing TNT mass. The TNT mass is fixed, the maximum deflection decreases with increasing POZD thickness, and the anti-explosion performance becomes better.

Due to the brittle characteristics of concrete, it is easy to produce cracks, collapses and other damage under strong dynamic loads such as explosion loads, resulting in cracks in the back of concrete and splash of concrete fragments. Compared with steel plate, corrugated steel can provide large out-of-plane stiffness, change the direction of shock wave propagation. It concentrates most of shock waves near the wave crest, reduces the stress concentration in other positions of slab, which is conducive to enhancing the bending strength and stiffness of the structure. POZD can absorb part of the energy generated

Table 2 Simulation results

No	POZD thickness /mm	TNT/g	Maximum deflection /mm	NO	POZD thickness /mm	TNT/g	Maximum deflection / mm
PSRC-1	6	500	0.99	PSRC-8	12	1000	6.90
PSRC-2		1000	12.91	PSRC-9		1500	22.65
PSRC-3		1500	35.86	PSRC-10		2000	47.89
PSRC-4		2000	68.26	PSRC-11		2500	62.20
PSRC-5		2500	76.96	PSRC-12		3000	63.23
PSRC-6		3000	89.20	PSRC-13		3500	70.16
PSRC-7		3500	103.77	PSRC-14		4000	91.00
PSRC-15	16	1000	6.58	PSRC-19	16	5000	69.54
PSRC-16		2000	17.73	PSRC-20		6000	88.88
PSRC-17		3000	38.22	PSRC-21		7000	104.10
PSRC-18		4000	57.10				

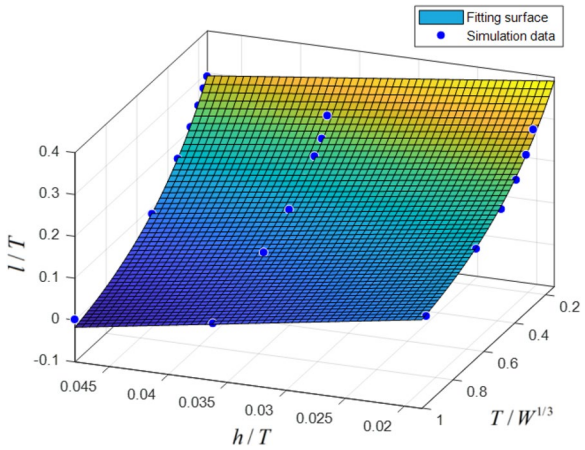

Fig. 10 The maximum deflection of the structure with different coating thickness under different TNT mass

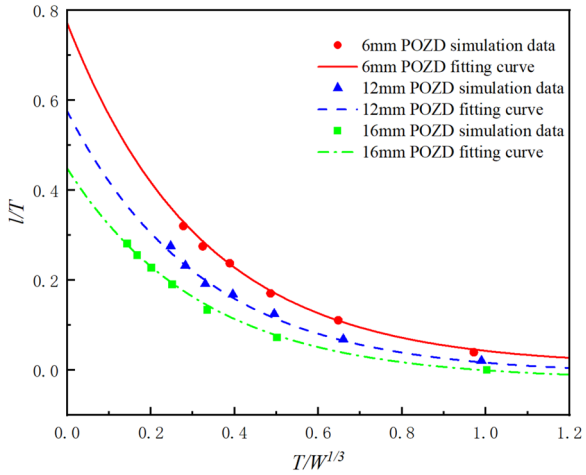

Fig. 11 Relationship between maximum deflection and TNT mass

by the explosion, thereby increasing the anti-explosion performance of the structure.

The dynamic response of PSRC slab under explosion is a complicated process. In order to explore its anti-explosion performance, combined with the numerical simulation results, the relationship between dimensionless deflection l/T and $T/W^{1/3}$ is fitted, as shown in Fig. 11. The fitting formula is as follows:

$$\begin{aligned}\frac{l}{T} =&(13.04\frac{h}{T}-1.23)\\ &\times(-0.77e^{-3.12T/W^{1/3}}-0.08)\\ &-0.07, 0.11\le\frac{T}{W^{1/3}}\le 1.23.\end{aligned}\tag{14}$$

In formula (14), when $T/W^{1/3}\le 0.11$, due to the small TNT charge, the shock waves cannot propagate to the bottom of the structure, and only a crater is formed on the front, as shown in Fig. 12(a). When $0.11\le T/W^{1/3}\le 1.23$, with the increase of explosive mass, the shock waves act on the bottom, causing the front crater, the back concrete spalling and POZD coating corrugated steel bulging deformation, as shown in Fig. 12(b). When $T/W^{1/3}\ge 1.23$, the energy generated far exceeds the load that the specimen can withstand, leading to the penetration failure of the entire structure, as shown in Fig. 12(c).

4.2 Influence of Corrugated Steel Angle

Based on the FE model in the third section, the blast resistance of PSRC slab is further studied by changing the corrugated steel angles and TNT mass while keeping the total thickness unchanged. The sketch of the model is shown in Fig. 13 and the program is shown in Table 3.

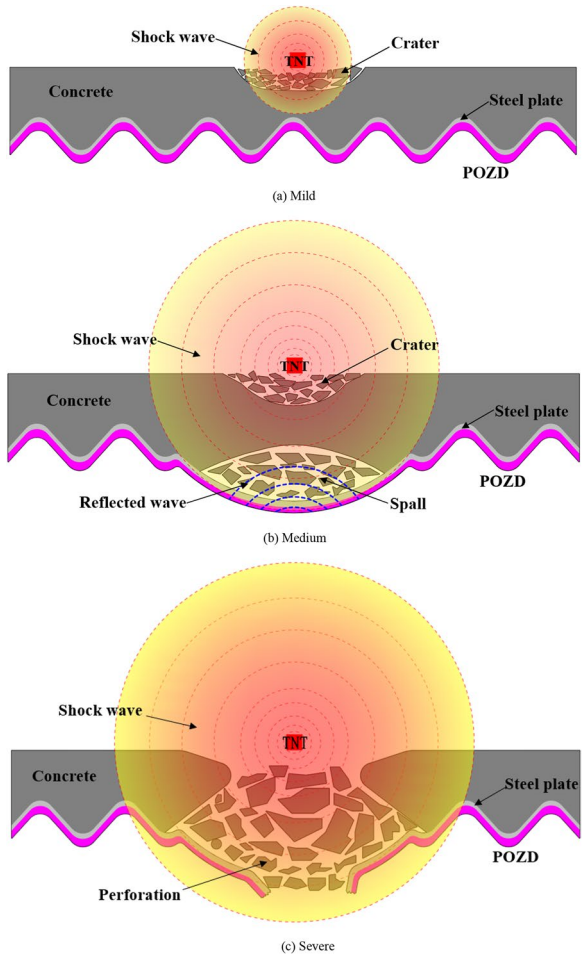

Fig. 12 Propagation of shock waves

In this section, the maximum deflection δ of PSRC slab was used as the criterion for structural failure. The relationship between δ and physical quantities can be expressed as follows:

$$\begin{aligned}\omega =& f(Q, \rho_e, E_e, \gamma_e; \rho_c, E_c, \nu_c, \sigma_c, D_c; \rho_s \\ & , E_s, \nu_s, \sigma_s, D_s; \rho_p, E_p, \nu_p, \sigma_p, D_p).\end{aligned} \tag{15}$$

In this paper, Q, ρ_e, E_e, γ_e are charge, density, energy per unit volume and expansion index of TNT; $\rho_c, E_c, \nu_c, \sigma_c, D_c$ are density, elastic modulus, Poisson's ratio, yield limit and thickness of concrete; $\rho_s, E_s, \nu_s, \sigma_s, D_s$ are density, elastic modulus, Poisson's ratio, yield limit and thickness of steel plate; $\rho_p, E_p, \nu_p, \sigma_p, D_p$ are density, elastic modulus, Poisson's ratio, yield limit and thickness of POZD.

When TNT, concrete and corrugated steel materials are selected consistently and structural size is determined, the charge Q, TNT density ρ_e and steel plate thickness D_s are taken as the basic quantities. Formula (16) can be converted into a simple dimensionless relation as follows:

$$\frac{\delta}{D_s} = f\left(\frac{\sqrt[3]{Q/\rho_e}}{D_s}\right). \tag{16}$$

According to the numerical simulation results in Table 3, $\frac{\sqrt[3]{Q/\rho_e}}{D_s}$ is taken as the abscissa, $\frac{\delta}{D_s}$ is taken as the ordinate, analyzing and fitting the data, the final fitting curve is shown in Fig. 12. The formula is as follows:

$$\begin{aligned}\frac{\delta}{D_s} =& (0.09 * (\frac{\theta\pi}{180})^{-1.6})\frac{\sqrt[3]{Q/\rho_e}}{D_s} \\ & - 72.41e^{-4\frac{\theta\pi}{180}}, 0 < \theta < 90^\circ, \\ & 0 < Q < 5000\end{aligned} \tag{17}$$

where θ represents the angle of corrugated steel.

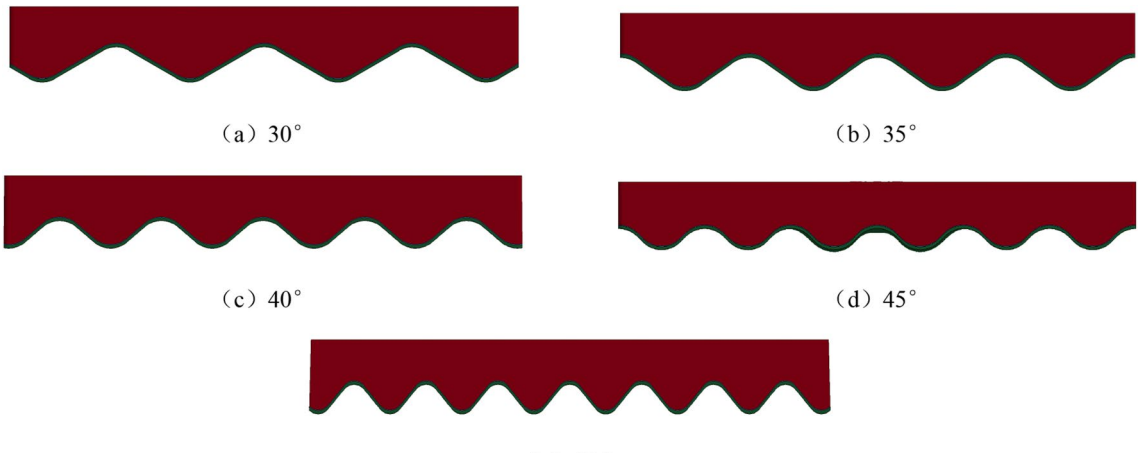

Fig. 13 Models of different corrugated steel angles. **a** 30°. **b** 35°. **c** 40°. **d** 45°. **e** 50°

Table 3 Numerical program

No	Angle of corrugated steel/°	TNT/g	Maximum deflection/mm
PSRC-22	30	1000	24.56
PSRC-23		1500	52.04
PSRC-24		2000	64.23
PSRC-25		2500	111.46
PSRC-26		3000	135.64
PSRC-27		3500	155.62
PSRC-28	35	1000	15.52
PSRC-29		1500	49.69
PSRC-30		2000	60.21
PSRC-31		2500	70.24
PSRC-32		3000	92.69
PSRC-33		3500	102.86
PSRC-34	40	1000	13.47
PSRC-35		1500	43.01
PSRC-36		2000	53.88
PSRC-37		2500	65.93
PSRC-38		3000	89.57
PSRC-39		3500	97.82
PSRC-40	45	1000	12.19
PSRC-41		1500	37.45
PSRC-42		2000	47.86
PSRC-43		2500	58.86
PSRC-44		3000	78.44
PSRC-45		3500	94.19
PSRC-46	50	1000	10.87
PSRC-47		1500	30.43
PSRC-48		2000	42.51
PSRC-49		2500	46.36
PSRC-50		3000	54.03
PSRC-51		3500	75.61

The maximum deflection increases approximately linearly with the increase of TNT mass. It can be seen from the numerical simulation results that when $\frac{\sqrt[3]{Q/\rho_e}}{D_s}$ is consistent, the maximum deflection decreases with increasing corrugated steel angles.

When the corrugated steel angle is 30 degrees, the $\frac{\delta}{D_s}$ of the specimen increases most obviously with the increase of the $\frac{\sqrt[3]{Q/\rho_e}}{D_s}$. When the angle is 35 degrees, 40 degrees and 45 degrees, the increasing trend of the $\frac{\delta}{D_s}$ decreases with the increase of the $\frac{\sqrt[3]{Q/\rho_e}}{D_s}$, but the difference is not obvious. When the angle of corrugated steel is 50 degrees, the growth rate of the $\frac{\delta}{D_s}$ is the lowest, as shown in Fig. 14. This shows that with the increase of corrugated steel angle, the PSRC slab blast resistance improvement effect will be better. When the angle is 50 degrees, the improvement effect of structural blast resistance is the best.

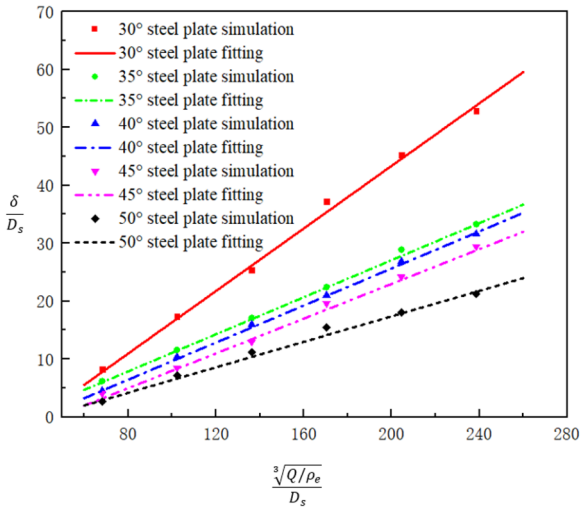

Fig. 14 Simulation data and fitting curve

5 Conclusion

In this paper, the effects of POZD and corrugated steel on the blast resistance of PSRC slab were investigated. The FE model was established by LS-DYNA software and the dynamic response process of the structure was studied. The effectiveness of the FE model was verified according to the test results. Then, the parametric analysis was conducted to investigate the influence of different POZD thicknesses and different corrugated steel angles on the structural damage effect. The conclusions are as follows:

(1) The dynamic response process of the structure was that the crater was first generated on the front of the structure, the concrete on the back was cracked. The concrete on the back was spalled, the POZD-coated steel plate produced slight bulging deformation. The spalling and bulging continued to expand until the structure was completely destroyed or the dynamic response process ended.
(2) Comparing the numerical simulation results with the experimental results, the errors of the bulge long diameter and bulge short diameter were 3.5% and 6.8%, respectively. The numerical model established in this paper can effectively simulate the damage process of PSRC under contact explosion.
(3) The POZD coating on the back of the structure made the peak stress of the stress wave generated by the explosion only 2.79% of the incident wave, which greatly weakened the energy propagation and improved the anti-explosion performance of the structure.

(4) The relationship between the back bulge height, the POZD thickness and $T/W^{1/3}$ was established. Based on the numerical results, the empirical expression of normalized bulge height considering both the POZD thickness and $T/W^{1/3}$ was obtained. The TNT mass was fixed, the maximum deflection decreases with increasing POZD thickness, and the anti-explosion performance became better.
(5) The empirical expression between the maximum deflection, corrugated steel angles and TNT mass was established. The anti-explosion performance of the structure increases with the increase of the corrugated steel angles, when the angle was 50 , the improvement effect of structural blast resistance was the best.

Further research on RC slabs strengthened with POZD-coated corrugated steel under contact explosive should be conducted. It is also necessary to study the influence of different reinforcement ratios and concrete strength and different strength of corrugated steel on the anti-explosion performance of the structure. The results of this paper will provide more basis for the application of PSRC slab in protection engineering.

Acknowledgements
The authors acknowledge the financial support from the National Natural Science Foundation of China (Grant Nos. 11302261 and 11972201). This paper is also supported by the project of Key Laboratory of Impact and Safety Engineering (Ningbo University), Ministry of Education. The project number is CJ202011.

Author contributions
Wei Wang: investigation, methodology, formal analysis, writing–original draft, writing–review and editing. Congkun Zhang: methodology, formal analysis, writing–original draft. Guangrui Yang: conceptualization, supervision, project administration.

Funding
This research was supported by the following fundings: The National Natural Science Foundation of China (Grant Nos. 11302261 and 11972201). The project of Key Laboratory of Impact and Safety Engineering of Ningbo University (Project No. CJ202011).

Availability of data and materials
All data generated or analyzed during this study are included in this published article.

Declarations

Ethics approval and consent to participate
We confirm that we attach sufficient importance to the protection of intellectual property rights related to this work and that there are no obstacles to publication in terms of intellectual property rights. We confirm that we have followed the provisions of our intellectual property agency.

Consent for publication
We confirm that the manuscript has been read and approved by all named authors. We confirm that the order of authors listed in the manuscript has been approved by all of us.

Competing interests
The authors declare that they have no known competing financial interests or personal relationships that could have appeared to influence the work reported in this paper.

Received: 5 May 2023 Accepted: 27 March 2024
Published online: 08 July 2024

References

Arman, B., Reddy, A. S., & Arya, G. (2012). Viscoelastic properties and shock response of coarse-grained models of multiblock versus diblock copolymers: insights into dissipative properties of polyurea. *Macromolecules, 45*(7), 3247.
Cheng, L., Ji, C., Gao, F., Yu, Y., Long, Y., & Zhou, Y. (2019). Deformation and damage of liquid-filled cylindrical shell composite structures subjected to repeated explosion loads: Experimental and numerical study. *Composite Structures, 220*, 386–401.
Chilvers, J., Yang, L., Lin, X., & Zhang, Y. X. (2022). Experimental and numerical investigations of hybrid-fibre engineered cementitious composite panels under contact explosions. *Engineering Structures, 266*, 114582.
Davidson, J.S., Sudame, S. and Dinan, R.J. (2004). Development of computational models and input sensitivity study of polymer reinforced concrete masonry walls subjected to blast.
Erduran, E., & Yakut, A. (2004). Drift based damage functions for reinforced concrete columns. *Computers & Structures, 82*, 121–130.
Ghodratian-Kashan, S. M., & Maleki, S. (2022). Experimental investigation of double corrugated steel plate shear walls. *Journal of Constructional Steel Research, 190*, 107138.
Gu, M., Ling, X., Wang, H., Dang, W., Teng, X., & Yu, A. (2022). Experimental investigation into dynamic mechanical properties and explosion responses of polyurea elastomer. *Process Safety and Environmental Protection, 163*, 144–157.
Gu, M., Ling, X.-D., Yu, A.-F., Chen, G.-X., Wang, H.-Z., & Wang, H.-X. (2021). Experimental study of polyurea-coated fiber-reinforced cement boards under gas explosions. *Defence Technology, 23*, 201.
Han, Z., Li, D., Zhou, T., Zhu, Q., & Ranjith, P. G. (2020). Experimental study of stress wave propagation and energy characteristics across rock specimens containing cemented mortar joint with various thicknesses. *International Journal of Rock Mechanics and Mining Sciences, 131*, 104352.
Haris, A., Lee, H. P., & Tan, V. (2018). An experimental study on shock wave mitigation capability of polyurea and shear thickening fluid based suspension pads. *Defence Technology, 14*(01), 14–20.
Ichino, H., Beppu, M., & Williamson, E. B. (2020). Blast-resistant performance of a two-stage concrete plate subjected to contact explosions. *Construction and Building Materials, 259*, 119766.
Iqbal, N., Sharma, P. K., Kumar, D., & Roy, P. K. (2018). Protective polyurea coatings for enhanced blast survivability of concrete. *Construction and Building Materials, 175*, 682–690.
Jin, S., Wang, Q., Zhou, J., & Bai, J. (2022). Experimental and numerical investigation of assembled multi-grid corrugated steel plate shear walls. *Engineering Structures, 251*, 113544.
Li, J., & Hao, H. (2014). Numerical study of concrete spall damage to blast loads. *International Journal of Impact Engineering, 68*, 41–55.
Li, J., Wu, C., Hao, H., Wang, Z., & Su, Y. (2016). Experimental investigation of ultra-high performance concrete slabs under contact explosions. *International Journal of Impact Engineering, 93*, 62–75.
Li, W., Li, F., & Chen, H. (2022). Performance of concrete-filled double-skin shallow-corrugated steel plate composite walls under axial compression. *Journal of Constructional Steel Research, 196*, 107374.
Liu, J., An, F.-J., Wu, C., Liao, S.-S., Zhou, M.-X., Xue, D.-Y., & Guo, H. (2022a). Experimental investigations on small-and full-scale ship models with polyurea coatings subjected to underwater explosion. *Defence Technology, 18*(7), 1257–1268.
Liu, J., Li, J., Fang, J., Liu, K., Su, Y., & Wu, C. (2022b). Investigation of ultra-high performance concrete slabs under contact explosions with a calibrated K&C model. *Engineering Structures, 255*, 113958.

Liu, J., Liu, C., Xu, S., Li, J., Fang, J., Su, Y., & Wu, C. (2022c). G-UHPC slabs strengthened with high toughness and lightweight energy absorption materials under contact explosions. *Journal of Building Engineering, 50*, 104138.
Malvar, L. J., Crawford, J. E., Wesevich, J. W., & Simons, D. (1997). A plasticity concrete material model for DYNA3D. *International Journal of Impact Engineering, 19*, 947–873.
Masahiro, M., Hideaki, T., Tomohiro, A., & Hiroyuki, H. (2004). Effects of concrete strength and reinforcing clear distance on the damage of reinforced concrete slabs subjected to contact detonations. *Concrete Research & Technology Japan Concrete Institute, 15*(2), 89–98.
Mcvay, M.K. *Spall Damage of Concrete Structures*
Shi, S., Liao, Y., Peng, X., Liang, C., & Sun, J. (2019). Behavior of polyurea-woven glass fiber mesh composite reinforced RC slabs under contact explosion. *International Journal of Impact Engineering, 132*, 103335.
Shi, Y., Hong, H., & Li, Z. X. (2008). Numerical derivation of pressure–impulse diagrams for prediction of RC column damage to blast loads. *International Journal of Impact Engineering, 35*(11), 1213–1227.
Shi, Y., Wang, J., & Cui, J. (2020). Experimental studies on fragments of reinforced concrete slabs under close-in explosions. *International Journal of Impact Engineering, 144*, 103630.
Song, K., Long, Y., Ji, C., Gao, F., & Chen, H. (2016). Experimental and numerical studies on the deformation and tearing of X70 pipelines subjected to localized blast loading. *Thin-Walled Structures, 107*, 156–168.
Sun, Z., Zou, Y., Wang, C., Pan, J., Wang, L., & Chen, M. (2022). Study on confinement mechanism of core concrete in steel tubular-corrugated steel plate confined concrete columns. *Journal of Building Engineering, 52*, 104497.
Wang, W., Huo, Q., Yang, J.-C., Wang, J.-H., & Wang, X. (2023). Experimental investigation of ultra-early-strength cement-based self-compacting high strength concrete slabs (URCS) under contact explosions. *Defence Technology*, 24, 326–3339. https://doi.org/10.1016/j.dt.2022.02.010
Wang, W., Huo, Q., Yang, J.-C., Wang, J.-H., Wang, X., & Gao, W.-L. (2021). Damage analysis of POZD coated square reinforced concrete slab under contact blast. *Defence Technology*. https://doi.org/10.1016/j.dt.2021.07.005
Wang, W., Liu, R., & Wu, B. (2014). Analysis of a bridge collapsed by an accidental blast loads. *Engineering Failure Analysis, 36*, 353–361.
Wang, W., Wang, Y., Yang, J., Wang, J., & Wang, X. (2022a). Investigation on air blast resistance of POZD-coated composite steel plates: Experiment and numerical analysis. *Composites Part b: Engineering, 237*, 109858.
Wang, W., Wei, G., Yang, J., Liu, F., & Gao, W. (2022b). Study on antiexplosion performance of reinforced concrete slabs strengthened with POZD coated steel plate under contact explosion. *Engineering Failure Analysis, 140*, 106589.
Wang, W., Yang, G., Yang, J., Wang, J., & Wang, X. (2022c). Experimental and numerical research on reinforced concrete slabs strengthened with POZD coated corrugated steel under contact explosive load. *International Journal of Impact Engineering, 166*, 104256.
Wang, W., Yang, J., Wang, J., Wang, X., & Huo, Q. (2021). Experimental investigation of polyisocyanate-oxazodone coated square reinforced concrete slab under contact explosions. *International Journal of Impact Engineering, 149*, 103777.
Wang, W., Zhang, D., Lu, F. Y., Tang, F. J., & Wang, S. C. (2013a). Pressure-impulse diagram with multiple failure modes of one-way reinforced concrete slab under blast loading using SDOF method. *Journal of Central South University, 20*(2), 510–519.
Wang, W., Zhang, D., Lu, F., Wang, S.-C., & Tang, F. (2012). Experimental study on scaling the explosion resistance of a one-way square reinforced concrete slab under a close-in blast loading. *International Journal of Impact Engineering, 49*, 158–164.
Wang, W., Zhang, D., Lu, F. Y., Wang, S. C., & Tang, F. J. (2013b). Experimental study and numerical simulation of the damage mode of a square reinforced concrete slab under close-in explosion. *Engineering Failure Analysis, 27*, 41–51.
Wu, G., Ji, C., Wang, X., Gao, F., Zhao, C., Liu, Y., & Yang, G. (2021). Blast response of clay brick masonry unit walls unreinforced and reinforced with polyurea elastomer. *Defence Technology*. https://doi.org/10.1016/j.dt.2021.03.004
Wu, G., Wang, X., Ji, C., Gao, Z., Jiang, T., Zhao, C., & Liu, Y. (2021). Anti-blast properties of 6063–T5 aluminum alloy circular tubes coated with polyurea elastomer: Experiments and numerical simulations. *Thin-Walled Structures, 164*, 107842.
Wu, J., Liu, Z., Yu, J., & Xu, S. (2022). Experimental and numerical investigation of normal reinforced concrete panel strengthened with polyurea under near-field explosion. *Journal of Building Engineering, 46*, 103763.
Xu, S., Chen, B., Li, Q., Zhou, F., Yin, X., Jiang, X., & Wu, P. (2022). Experimental and numerical investigations on ultra-high toughness cementitious composite slabs subjected to close-in blast loadings. *Cement and Concrete Composites, 126*, 104339.
Yang, M., Tian, L., Yuan, Y., & Yang, Z. (2021). The study on composite trough beam with corrugated steel web wrapped with steel plate: Experiment and bending properties. *Journal of Constructional Steel Research, 185*, 106853.
Yong, L., Wang, Z., & Chong, K. (2005). A comparative study of buried structure in soil subjected to blast load using 2D and 3D numerical simulations. *Soil Dynamics and Earthquake Engineering, 25*(4), 275–288.
Yu, X., Zhou, B., Hu, F., Zhang, Y., Xu, X., Fan, C., Zhang, W., Jiang, H., & Liu, P. (2020). Experimental investigation of basalt fiber-reinforced polymer (BFRP) bar reinforced concrete slabs under contact explosions. *International Journal of Impact Engineering, 144*, 103632.
Zhang, J.-L., Liu, B.-D., & Liu, R. (2021). Behavior of sinusoidal-corrugated-steel-plate–concrete composite slabs: Experimental investigation and theoretical model development. *Journal of Constructional Steel Research, 187*, 106958.
Zhang, L., Ji, C., Wang, X., Wang, Y., Wu, G., Zhu, H., & Han, Z. (2022). Strengthening and converse strengthening effects of polyurea layer on polyurea–steel composite structure subjected to combined actions of blast and fragments. *Thin-Walled Structures, 178*, 109527.
Zhao, C., Lu, X., Wang, Q., Gautam, A., Wang, J., & Mo, Y. L. (2019). Experimental and numerical investigation of steel-concrete (SC) slabs under contact blast loading. *Engineering Structures, 196*, 109337.
Zhu, H., Wang, X., Wang, Y., Ji, C., Wu, G., Zhang, L., & Han, Z. (2022). Damage behavior and assessment of polyurea sprayed reinforced clay brick masonry walls subjected to close-in blast loads. *International Journal of Impact Engineering, 167*, 104283.
Zuo, J.-Q., Zhu, B.-L., Guo, Y.-L., Wen, C.-B., & Tong, J.-Z. (2022). Experimental and numerical study of steel corrugated-plate coupling beam connecting shear walls. *Journal of Building Engineering, 54*, 104662.

Publisher's Note

Wei Wang is a Professor in the Key Laboratory of Impact and Safety Engineering of Ministry of Education and Institute of Advanced Energy Storage Technology and Equipment at Ningbo University. His research direction is impact dynamics.

Congkun Zhang is a Graduate student in the Key Laboratory of Impact and Safety Engineering of Ministry of Education at Ningbo University.

Guangrui Yang is a former graduate student in the Key Laboratory of Impact and Safety Engineering of Ministry of Education at Ningbo University.